Optics of perovskite solar cell front contacts

Mohammad I. Hossain[1], Aswin Hongsingthong[2], Wayesh Qarony[1], Porponth Sichanugrist[2], Makoto Konagai[2,3], Alberto Salleo[4], Dietmar Knipp[4,*], Yuen H. Tsang[1,*]

1.) Department of Applied Physics and Materials Research Center, The Hong Kong Polytechnic University, Hung Hom, Kowloon, Hong Kong

2.) Department of Physical Electronics, Tokyo Institute of Technology, Tokyo, Japan

3.) Photovoltaics Research Center (PVREC), Tokyo Institute of Technology, Tokyo, Japan

4.) Geballe Laboratory for Advanced Materials, Department of Materials Science and Engineering, Stanford University, Stanford, CA 94305, USA

*Corresponding authors: E-mail: yuen.tsang@polyu.edu.hk (Y. H. Tsang), dknipp@stanford.edu (D. Knipp)

ABSTRACT

The front contact has a major impact on the electrical and optical properties of perovskite solar cells. The front contact is part of the junction of the solar cell, must provide lateral charge transport to the terminals, should allow for an efficient light incoupling, while having low optical losses. The complex requirements of perovskite solar front contact will be described, and the optics of the front contact will be investigated. It will be shown that the front contact has a distinct influence on the short circuit current and energy conversion efficiency. Metal oxide films were investigated as potential front contacts. The incoupling of light in the solar cell is investigated by Three-dimensional Finite Difference Time Domain optical simulations and optical

measurements of experimentally realized self-textured zinc oxide films. The zinc oxide films were prepared by metal-organic chemical vapor deposition at low temperature. Furthermore, the influence of free carrier absorption of metal oxide films on the optics of low bandgap and/or tandem solar cells is investigated. Guidelines are provided on how to choose the doping concentration and thickness of the metal oxide films. Finally, it will be shown that by selecting an optimal front contact design the short circuit current and energy conversion efficiency can be increased by at least 15%.

1. Introduction

In recent years, the perovskite material system has gained considerable attention because of its ability to tailor the bandgap, its low deposition temperature, and most importantly, its excellent electronic and optical properties. The low penetration or absorption depths of several tens to hundreds of nanometers in combination with the high diffusion lengths >1 μm allows for realizing thin film solar cells with high energy conversion efficiency.[1–7] Single-junction solar cells with energy conversion efficiencies exceeding 20% have been demonstrated by several research groups.[8,9] Furthermore, the tunable optical bandgap of perovskites allows for realizing efficient multi-junction solar cells.[2,9–15]

However, so far, most emphasis has been on the optimization of the absorber material and the electronic properties of the contact layers of the solar cells. Little emphasis has been on the optics of the solar cell and the influence of the contact layers on the optics of the solar cells. However, the optics of the contact layers has a distinct influence on the optics of the complete solar cells and the short circuit current. The optics of the contact layers is important for single junction solar cells and even more

important for multijunction solar cells like perovskite/silicon tandem solar cells. The front contact of a perovskite solar cell has four functions. Firstly, the front and back contact together with the perovskite absorber form the junction of the solar cell. Hence the work function of the materials must be selected accordingly. Secondly, the front contact must provide lateral conductivity, so that the charges can be transported to the solar cell terminals or a printed metallic front contact grid. Thirdly, the front contact must allow for an efficient incoupling of the light in the solar cell. It might be combined with the diffraction or refraction of the incident light to increase the optical path length of the light in the solar cell, which results in an increased quantum efficiency. Often this is achieved by texturing of the contacts. Fourthly, the absorption loss of the contact layer should be as low as possible. The second point is closely linked to the fourth point. An increased doping concentration leads to an increased conductivity, but also the free carrier absorption is increased and potentially the absorption loss of the contact layers is increased. The aim of the study is to propose a solar cell design that allows for reaching short circuit current of more than 90% of its maximum short circuit currents. Such high values have been achieved for record silicon or gallium arsenide solar cells exceeds 90% of the theoretical limit.[16,17] In the case of perovskite solar cells, such high values have not been achieved yet.

2. Perovskite Solar Cell Structure

Most research on perovskite solar cells is still focused on single junction solar cells. However, the combination of perovskite and silicon as part of a perovskite/silicon tandem solar cell exhibits the largest economic potential, because this combination allows for reaching high energy conversion efficiencies, while the manufacturing cost is low.[18–22] In this case, the perovskite solar cell must be integrated on a crystalline silicon wafer-based bottom solar cell. Hence, we will focus on device structures in

substrate configuration, opposite to solar cells on glass substrates, commonly referred to as solar cells in superstrate configuration.

The refractive index of the perovskite material system is comparable to the refractive index of the metal oxide contact layers. Hence, reflections at the metal oxide/perovskite interface are low. The reflection of two materials forming a planar interface increases with increasing refractive index difference between the materials. Hence the layer stack consisting of the metal oxide layers and the perovskite layer can be treated like one unit with almost equal refractive index. This simplifies the optical design. Hence, we can focus on the coupling of the incident light in the solar cell. This can be achieved by integrating a pyramidal surface texture on top of the solar cell. Depending on the dimensions of the pyramidal texture the structure might as well diffract or refract the incident light, so that the optical path length is increased. Consequently, the electrical properties of the solar cells should be comparable to planar perovskite solar cells realized in substrate configuration. It is assumed that the modified optical design does not affect the electrical properties of the solar cells. Hence it can be expected that the electrical parameter of the solar cell, the open-circuit voltage and fill factor, are comparable to planar solar cells in substrate configuration.

Cross sections of perovskite solar cell with smooth and textured front contact are depicted in Fig. 1(a,b). The photon management in perovskite solar cells differs fundamentally from photon management in silicon thin film and silicon wafer-based solar cells. Silicon exhibits a distinctly higher refractive index than perovskite, so that the interface between the silicon diode and the metal oxide contact layers must be textured to allow for an efficient photon management.

Nickel oxide (NiO) and zinc oxide (ZnO) layers are used as hole transporting/electron blocking and electron transporting/hole blocking layers, respectively. It is difficult to realize NiO films with high transmission and high conductivity. Hence a 5 nm NiO layer

in combined with a 75 nm thick ITO is used as a contact. Such a double layer of NiO and ITO is used to combine hole transporting/electron blocking with high transmission and low lateral resistivity. It is assumed that the NiO/ITO double layer forms a tunnel junction. The selected double layer is consistent with layer stacks used by several experimental studies on perovskite solar cells in the superstrate configuration.[23,24] The formation of a front contact on top of the perovskite absorber is complex. A variety of materials and material combinations have been investigated. Zinc oxide films have been prepared by spin coating from ZnO nano particle solutions, resulting in solar cells with high energy conversion efficiency.[25] Other authors prepare a C_{60} layer prior to preparing a ZnO film, or a lithium fluoride (LiF) layer followed by a C_{60} and a zinc oxide layer. The C_{60} and LiF layers are introduced to control the work function and prevent the damage of the underlying perovskite layer. We have investigated the influence of different front contact configurations on the optics of the solar cells. The simulation results are provided in the supplementary material. The C_{60} layer causes absorption losses and a distinct drop of the quantum efficiency is observed. The LiF layer has almost no influence on the quantum efficiency if the LiF layer is placed between the perovskite and the C_{60} layer. The LiF causes only a distinct reflection loss if the LiF is placed between the perovskite and the ZnO layer and the C_{60} layer is removed (Fig. S2). However, such structure has not been proposed as a potential contact configuration. The corresponding simulations are provided in Fig. S2 of the supplementary document. Even though the C_{60} layer leads to a distinct drop of the quantum efficiency the C_{60} layer has no influence on the proposed ideas and conclusions. Hence, we focused in the following on a solar cell with only a ZnO contact layer. An aluminum layer is used as back contact and back reflector. Furthermore, the influence of an encapsulation layer on the solar cell was not considered. Further

information on the influence of an encapsulation layer on the optics of the solar cell is provided in Fig. S3 of the supplementary material.

Figure 1

3. Photon management

The perovskite device structure in Fig. 1(b) allows for an enhancement of the energy conversion efficiency by using a different front contact design. On one hand the dimensions of the front contact texture must be derived and on the other hand, it must be possible to fabricate such structures. In section 3(a) the fabrication of such surface textures by a self-texturing process is investigated. Such self-texturing has been successfully used to increase the short circuit current and energy conversion efficiency of silicon thin film solar cells. However, such self-textured contacts have not been investigated as potential front contacts of perovskite solar cells. Optical simulations to determine the optimal dimensions of the front contact are provided in section 3(b).

a) Experimental realization of textured metal oxide contact layers

Textured zinc oxide layers doped with aluminum, gallium or boron can be realized by a variety of deposition methods. Zinc oxide films with pyramidal or inverted pyramidal structure have been realized by chemical vapor deposition, pulse laser deposition or the wet chemical etching of sputtered zinc oxide films in diluted solutions of hydrochloric or hydrofluoric acids.[26–31] This study focuses on films prepared by chemical vapor deposition.[26–28] The chemical vapor deposition of textured metal oxide films is a standard process used in industry to coat several square meter large glass substrates.[32,33] As a part of this study boron-doped zinc oxide (ZnO:B) film were prepared by a Metal-Organic Chemical vapor deposition (MOCVD) process. The ZnO

thin films are deposited on Corning 7059 glass substrates using Diethylzinc ($C_4H_{10}Zn$) as a precursor and a mixture of heavy (D_2O) and "light" water (H_2O) as oxidants. Diborane (B_2H_6) (1% H_2 diluted) was used as a dopant gas. The films were grown at substrate temperature and pressure of 160 °C of 3 Torr, respectively. The surface morphology of the ZnO films can be controlled by the D_2O/H_2O ratio. The D_2O/H_2O ratio was varied from 0 to 1. The thickness of the zinc oxide films was kept constant at about 1.6 μm. Fig. 1(c) exhibits a Scanning Electron Microscope (SEM) image of a smooth boron-doped zinc oxide film, while Fig. 1(d) shows a boron doped film that is covered with quasi-randomly arranged pyramids. Fig. 1(c) exhibits the SEM of a film prepared by using a D_2O/H_2O ratio of 1, while the D_2O/H_2O ratio is 0 for the film shown in Fig. 1(d). The size of the pyramids can be controlled by the thickness of the zinc oxide film. The size of the pyramids increases with increasing thickness the ZnO film. Each pyramid can be characterized by a period, p, and a height, h. The opening angle of the pyramid is given by 2×tan(p/2/h). Small pyramids exhibit an opening angle of 135°-140° corresponding to the opening angle of inverted pyramids etched in zinc oxide single crystals. With increasing film thickness and increasing size of the pyramids the opening angle decreases.[26,34] Opening angles down to 40° have been observed for ZnO films with a thickness of up to 7 μm.[35] The films fabricated as part of this study exhibit a charge carrier concentration of 2×10^{20} cm^{-3} irrespective of the D_2O/H_2O ratio. For D_2O/H_2O ratios of 0 and 0.1 the electron charge carrier mobility is 15 $cm^2/V/s$, while for higher D_2O/H_2O ratios ranging from 1 to 10 the electron charge carrier mobility is approx. equal to 7.5 $cm^2/V/s$. Fig. 2(a) exhibits the total (specular plus diffuse) transmission of the films. The averaged total transmission for all films is higher than 80% in the spectral range from 400 nm to 800 nm. The haze in transmission is shown in Fig. 2(b). The haze is defined as the diffuse transmission normalized to the total

transmission. The haze increases with decreasing D_2O/H_2O ratio and increasing roughness of the ZnO film.

With increasing haze more light is diffracted by the texture of the ZnO film. However, the haze does not provide information on the diffraction angle of the diffracted light. Furthermore, it is difficult to directly correlate haze measurements with the quantum efficiency and short circuit current of solar cells. Optical simulations allow for a good correlation of the surface texture and the quantum efficiency.

Figure 2

b) Optical simulation

The refractive index of the used zinc oxide and ITO is depicted in Fig. 3(a) along with the refractive index of perovskite (methylammonium-lead(n)-iodide, $CH_3NH_3PbI_3$ ($MAPbI_3$)) material used in the investigation. The refractive index of the ZnO and ITO layers is comparable with the refractive index of the perovskite material. The perovskite material system exhibits a high absorption coefficient and, hence, a low absorption or penetration depth. The penetration depth ($t_p = 1/\alpha_p(\lambda)$) is the inverse of the absorption coefficient and defined as the thickness at which the incident light intensity drops to $1/e$. The dashed lines added to the graph represent the penetration depth for a solar cell with a 100 nm and 400 nm thickness as shown in Fig. 3(b). The incident light is absorbed up to a wavelength of 610 nm and 770 nm assuming a penetration depth of 200 nm and 800 nm, respectively. The optical data used in this study was adapted from the literature.[36–39]

Figure 3

We used the Finite Difference Time Domain (FDTD) simulations to calculate the 3D optical wave propagation. Details on the method and procedures to calculate power density profiles, the quantum efficiency, and the short circuit current are provided in previous publications and the supplementary material.[40,41] The optical wave propagation was investigated for pyramids with heights of 200 nm, 400 nm, and 600 nm while the period is varied from 150 nm to 1200 nm. The pyramids are formed on a continuous layer of ZnO. In the case of an experimentally realized solar cell, the thickness of the continuous layer is determined by the doping concentration, which is linked to the required lateral sheet resistance of the ZnO layer and the growth conditions of the ZnO film. The influence of the thickness of the continuous layer on the quantum efficiency and short circuit current is shown in Fig. S4. The absorption losses of the continuous ZnO layer increase with increasing thickness of the film. However, the thickness has no influence on the light incoupling of the solar cell and the light trapping of the solar cell. In the following, it is assumed that the ZnO layer has a thickness of 400 nm, while the period and height of the surface texture are 600 nm and 600 nm. Fig. 4 exhibits a comparison of external quantum efficiency and total reflection of a pyramidal textured and flat perovskite solar cell with an absorber thickness of 100 nm and 400 nm, respectively.

The quantum efficiency of the planar solar cell is characterized by pronounced interference fringes. The 400 nm thick ZnO front contact is responsible for the formation of interference fringes. As compared to the flat solar cell, the pyramidal textured solar cell shows a higher quantum efficiency throughout the complete spectral range for the 100 nm and 400 nm thick perovskite solar cell. For short wavelengths, the absorption coefficient of the perovskite material is very large, and the penetration depth is very small. Hence, the penetration depth is smaller than twice the thickness of the absorber of the solar cell. For a 100 nm thick solar cell, the penetration depth is

equal to twice the absorber layer thickness for a wavelength of 580 nm, while for a solar cell with an absorber thickness of 400 nm the transition point is shifted to 770 nm. The gain of the quantum efficiency is caused by an improved incoupling of light in the solar cell. Hence it can be concluded that for short wavelengths light trapping of the incident light does not lead to an increased quantum efficiency. The light might be diffracted by the surface texture, but the diffraction does not lead to increased light absorption. The light is absorbed irrespective of the diffraction of the incident light. For $t_p > 2 \times d$, the situation is different. The penetration depth is larger than two times the thickness of the perovskite absorber and the gain in the quantum efficiency is caused by improved incoupling and increased absorption of the incident light due to diffraction. This is also confirmed by the calculated total reflection of the solar cells in Figs. 4(c) and 4(d). The total reflection is calculated by $R = 1 - A_{total}$, where A_{total} is the total absorption of the solar cell. The total absorption of the solar cells approaches unity if the pyramid texture allows for an efficient incoupling and $2 \times d > t_p$, which occurs for wavelengths up to 580 nm and 770 nm using 100 nm and 400 nm thick perovskite absorber layers, respectively. For $2 \times d < t_p$ the total absorption is distinctly increased, due to the improved incoupling and light trapping, but the total absorption does not approach unity.

Figure 4

It should be noted here that the roughness of the perovskite films is not considered in the optical simulations. The roughness of the perovskite film depends on several factors like the deposition method, the temperature during the deposition and temperatures during potential subsequent deposition steps or annealing procedures. As previously mentioned, the refractive index of the metal oxide contact layers and the

perovskite layer is comparable. Hence a rough interface will have only a very small effect on the optics. It can be expected that the effect of the roughness on the electronic properties is distinctly larger. Only for the planar reference solar cell shown in Fig. 1(a) the interference fringes will be reduced, while the short circuit current is not affected. In the case of the solar cell structure in Fig. 1(b) most light propagation is incoherent, so that the quantum efficiency and the short circuit current are not affected.

Figure 5

In the following, the influence of the dimension of the pyramidal surface texture on short-circuit current density is studied. Again, the thickness of the perovskite layer was set to 100 nm and 400 nm. Fig. 5(a-c) exhibit the short circuit current density for an absorber layer thickness of 100 nm, while the short circuit current density plots for a thickness of 400 nm are shown in Fig. 5(d-f). Three different pyramid texture heights (200 nm, 400 nm, and 600 nm) are considered for the investigations, while for each height the period of the pyramid is varied from 150 nm to 1200 nm. Fig. 5(a,d) exhibit the total short circuit current density of the 100 nm and 400 nm thick solar cells as a function of the period of the surface texture. Short and long dashed lines are added to the graphs. The long-dashed line corresponds to the short circuit current density of a flat solar cell as shown in Fig. 1(a). The short-dashed line exhibits the short circuit current density of a flat solar cell assuming perfect incoupling of the light in the solar cell. Fig. 5(a,d) shows that the short circuit current density of the textured solar cell is always larger than the short circuit current of the flat solar cell irrespective of the selected height and period. For small periods of the pyramid texture, $n_{ZnO} \times p_{ZnO} << \lambda$, the pyramidal texture acts like a refractive index gradient, which allows for efficient light incoupling in the solar cell. With increasing period, the incident light is diffracted, so

that a further increase of the short circuit current is observed. The short circuit current density increases with increasing height of the pyramid. In other words, the opening angle of the pyramid, which is given by $2 \times \tan(p/2/h)$, decreases with increasing height of the pyramid. For large opening angles, which are reached for small pyramid heights and larger periods, the incident light is diffracted in small angles. Consequently, the short circuit current density drops below the short circuit current density of a solar cell exhibiting perfect incoupling of light and converges towards the short circuit current density of a flat solar cell. The highest short circuit current density is achieved for a period of the pyramid texture of approximately 500 nm. In the case of the thin perovskite solar cell (100 nm absorber), the short circuit current density is increased from 13.8 to ~18.5 mA/cm^2. The short circuit current density of the thick solar cell (400 nm) is increased from 20.6 to ~23.6 mA/cm^2. This corresponds to a relative short circuit current density gain of 34% (100 nm) and 14.5% (400 nm). The short circuit current gain is defined as $(I_{SC\_tex}-I_{SC\_flat})/I_{SC\_flat}$, where I_{SC_tex} and I_{SC_flat} are the short circuit current of the textured and the reference planar (flat) solar cell. For the thin solar cell, a distinct gain of the short circuit current density is achieved due to the increased absorption caused by diffraction, while for the thick solar cell the absorption is only slightly increased. For this structure, the diffraction of the light has only a small effect on the total short circuit current density. In order to separate the effect of light incoupling from light trapping, the short circuit current density is divided. Fig. 4(b,e) exhibits the short circuit current density up to the wavelengths where $t_p=2 \times d$, which is 580 nm and 770 nm. Up to this wavelength, the gain in the short circuit current is caused by an improved light incoupling. For longer wavelengths, diffraction has an additional effect on the short circuit current density. The short circuit current density plots for longer wavelengths are shown in Fig. 5(c, f). For the thin solar cell (Fig. 5(c)), a large absolute gain of the short circuit current density is observed, while the relative

gain of the short circuit current is small. The absolute short circuit current is increased by approx. 3 mA/cm^2 for an optimal period. However, the relative gain of the short circuit current is smaller than 100%. For the thick solar cell, diffraction has only a small effect on the absolute short circuit current density. Hence, the total short circuit current density gain is small, while the relative short circuit current gain is large. The absolute short circuit current is increased by approx. 0.8 mA/cm^2 for an optimal period. However, the relative gain of the short circuit current is approx. 400%.

The influence of the period of the surface texture on the power density map is shown in Fig. 6. The power density profiles of 100 nm and 400 nm thick perovskite solar cells are shown in Fig. 6 for an incident wavelength of 700 nm. Surface textures with a period of $n_{ZnO} \times p_{ZnO} << \lambda$, allow for an efficient light incoupling in the solar cells, while for larger periods light trapping is observed. The optical simulations are carried out for periods of 300 nm and 900 nm, while the height is kept constant at 600 nm. For the case of 300 nm period, a standing wave is formed in the solar cell as depicted in Fig. 6 (a) and Fig. 6(b). The standing wave indicates that the pyramids act as a refractive index grating. The light is not diffracted by the pyramids. Whereas, the incident light is diffracted by the pyramid for surface textures with a period of 900 nm. Consequently, a distinctly higher power density is observed for perovskite solar cells with large surface texture irrespective of perovskite absorber layer thickness. This is confirmed by the power density profile shown in Fig. 6(c) and Fig. 6(d).

Figure 6

The short circuit current density as a function of the solar cell thickness is shown in Fig. 7(a) for a small (300 nm) and large (900 nm) period. Again, the solar cell on a smooth surface is used as a reference cell here. Furthermore, the short circuit current

density gain is plotted in Fig. 7(b). For thick perovskite absorber layers, both solar cells with small and large surface texture reach equal short circuit current densities. A relative short-circuit current density gain of 12.5% is observed. This gain is mainly caused by the improved light incoupling. Very good incoupling is observed for the small and large surface texture. For thin solar cells, the additional diffraction of the incident light leads to an additional gain of the short circuit current density. For the investigated solar cells, a short circuit current density gain of up to 25% is observed.

The calculated short circuit current density for the solar cell with the 400 nm thick absorber reaches 90% of the upper theoretical short circuit current limit of 25.6 mA/cm^2. The almost perfect incoupling can be achieved by using a surface texture, where $n_{ZnO} \times p_{ZnO} << \lambda$. In this case, the height of the pyramid texture must be $h_{ZnO} \geq \lambda/2/n_{ZnO}$. Even for the larger periods, an almost perfect light incoupling can be achieved. The opening angle of the pyramid should be 50° or smaller to achieve an effective light incoupling. Zinc oxide pyramids with such small opening angles can only be fabricated by growing thick ZnO films with large pyramids. Hence good incoupling can experimentally only be achieved by growing large pyramids and thick zinc oxide films.

Figure 7

4. Conductivity versus optical losses

The absorption loss of the contact layer should be as low as possible, while the conductivity of the contact layers should be as high as possible. However, these two aims contradict each other. By minimizing the lateral resistivity of the contact layers the series resistance is reduced and the fill factor is maximized. If the doping concentration of the metal oxide layer is low the series resistance is increased and the

fill factor is lowered, so that finally the energy conversion efficiency is negatively affected. On the other hand, the free carrier absorption of the contacts layer is low if the doping concentration of the metal oxide film is low. Hence a low doping concentration allows for a high short circuit current.

Most perovskite solar cells are prepared in superstrate configuration on thin but highly doped ITO (Indium tin oxide) front contacts. The transmittance (T), absorbance (A), and reflectance (R) of a typical planar metal oxide layer (zinc oxide) is shown in Fig. 8. An extended Drude Lorentz model was used to describe the complex refractive index of the metal oxide film.[36,37] The spectra can be divided in four regions. a.) the direct band-to-band absorption region for short wavelengths, b.) The transparent region covering the visible and near infrared part of the optical spectrum and c.) the free carrier absorption region. The free carrier region can be described by the plasma wavelength λ_p and finally, d.) the reflection state. The relationship between the doping concentration and the plasma wavelength can be described by

$$\lambda_p = \frac{2\pi \times c}{q} \sqrt{\frac{\varepsilon_0 \varepsilon_\infty m^*}{N_{Opt}}} \qquad (1)$$

where, c is the speed of light in space, m^* is the effective mass of the electron, ε_0 and ε_∞ are the vacuum and relative permittivity of the metal oxide film, respectively. With increasing doping concentration, the plasma wavelength shifts to shorter wavelengths. In the case of a perovskite single junction solar cell a thin and highly doped metal oxide film can be selected. The absorption loss due to free carrier absorption is usually low. For a multi-junction solar cell, like a perovskite/silicon tandem solar cell, the situation is different. The free carrier absorption might have a negative effect on the quantum efficiency for long wavelengths. Fig. 9 exhibits the optical simulation of a

perovskite/silicon tandem solar cell. Details on the calculation of the quantum efficiency are provided in Ref. 18. A tandem solar cell with a continuous ZnO front contact layer is compared to a tandem solar cell with a continuous ITO layer with equal conductivity. An extended Drude Lorentz model was used to describe the complex refractive index of ZnO and ITO. The model used to calculate the optical constants is provided in the supplementary material. The calculated complex refractive indices were compared to experimentally determined optical constants and a good agreement was observed. The ZnO layer has a thickness of 400 nm, while the thickness of the ITO layer is only 70 nm. The parameters used for calculating the complex refractive index are provided in the supplementary material, in Tab. S1.

The tandem solar cell design shown in Fig. 9(a) was previously investigted and compared to a design with textured interfaces. We call the solar cell in Fig. 9(a) and 9(b) an optically rough but electrically smooth solar cell, oppose to a completely textured solar cell, which is optically and electrically rough. Both solar cells provide almost equal short circuit current densities of close to 20 mA/cm^2. Here we have compared the ZnO font contact with a ITO layer with equal conductivty. Due to the higher doping concentration of the ITO layer a distinctly higher absorption of the front ITO layer is observed as shown in Fig. 9(d). The optical loss increases from 1.65 mA/cm^2 to 2.5 mA/cm^2, while the total short circuit current drops to approximately 19 mA/cm^2. It can be concluded that high doping concentrations and thin metal oxide front contacts can be used for solar cells using materials with large bangaps, while for low bandgap solar cells or multijunction solar cells the doping concentration should be reduced and the thickness of the front contact should be increased to limit the optical losses of the front contact.

5.   Towards optimal front contacts of perovskite solar cells

The front contacts of perovskite single and multi-junction solar cells in substrate configuration must fulfill several requirements as already pointed out in the introduction. Firstly, the front and back contact together with the perovskite absorber form the junction of the solar cell. Hence the work function of the materials must be selected accordingly. Secondly, the front contact must provide a high lateral conductivity, so that charges can be transported without significant ohmic losses. Thirdly, light must be efficiently coupled in the solar cells, and fourthly, the absorption loss of the contact layer should be as low as possible.

It is difficult for one layer to fulfil all these requirements. Hence, we propose a multi-layer system consisting of three layers. The layers and the function of the individual layers will be described in the following.

I.) High work function and protection layer

The first layer must be directly prepared on the perovskite layer. The work function of the material should be matched to the band structure of the perovskite film to allow for a high open circuit voltage. The layer can be thin but should prevent the damage of the under lying perovskite layer due to the subsequent deposition of layer II and III. The layer might be formed by zinc oxide or other materials. The optical losses of this layer should be low as the layer should be very thin.

II.) Lateral charge transport layer with low optical losses

The layer should provide a high lateral conductivity, so that charge can be transported to the external terminals or printed front contact grid of the solar cell. At the same time the optical loss of the layer should be low. For wide bandgap material single junction solar cells this can be achieved by thin and highly doped metal oxide films, like the commonly used ITO. For low bandgap materials and multi-junction solar cells the doping concentration

must be lower to prevent absorption losses due to free carrier absorption. Subsequently metal oxides with high charge carrier mobility like hydrogen doped indium oxide (IOH) or thick metal oxide films must be used.[42,43] It can be expected that the optical loss of the complete front contact layer system is determined by this layer.

Incoupling and/or light trapping layer

The layer allows for an efficient coupling of the light in the solar cell. Depending on the needs the layer might also diffract the light to increase the optical path length. Again, such structures can be realized by using metal oxides. For example, a self-texturing ZnO films prepared by MOCVD can be used. In the case of a perovskite single junction solar cell or an all-perovskite multi-junction solar cells the film does not have to be doped. In the case of a perovskite/silicon tandem solar cell as shown in Fig. 9, the film must be doped, because the metal front contact grid must be printed on the multi-layer front contact.

If the perovskite is directly deposited on a textured silicon wafer as part of a perovskite/silicon tandem solar cell layer I and II are required, but the layer III is not required anymore.

6. Summary

The optics of perovskite single junction and perovskite/silicon tandem solar cell front contacts has been studied. Metal oxide films were used as front contacts with refractive indices ($\cong 2.2$) comparable to the perovskite material system ($\cong 2.5$). Hence the solar cell with contacts can be treated as one unit and the optics of the solar cell is largely affected by the optics of the front contact. An optimized front contact of the solar cell consists of a multi-layer of three films with different functions. The first layer with a well-

tailored work function is responsible for forming the junction and prevent the damage of the perovskite layer due to subsequent deposition steps. The second layer provides the lateral charge transport to the terminals or a printed metal grid. For wide bandgap material single junction solar cells this can be achieved by thin and highly doped metal oxide films. For low bandgap materials and multi-junction solar cells the doping concentration must be reduced to prevent absorption losses due to free carrier absorption. Subsequently metal oxides with high charge carrier mobility or thick metal oxide films must be used. The third layer is responsible for the incoupling and potentially diffraction of the incident light. Such function can be implemented by using self-textured zinc oxide films prepared by metal-organic chemical vapor deposition. The surface morphology of the ZnO films can be controlled by the heavy (D_2O) to "light" water (H_2O) ratio during the deposition. Efficient light incoupling is achieved, if the opening angle of the pyramids is smaller than 50°. The size of experimentally realized pyramid textures can be controlled by the growth conditions and the film thickness. Pyramids with small opening angles can be realized by using thick ZnO films and large pyramids. Optical simulations shown that an improved optics of the front contact leads to short circuit current density gain from 13.8 to ~ 18.5 mA/cm^2 and 20.6 to ~23.6 mA/cm^2 in the case of thin (100 nm absorber) and thick (400 nm absorber) perovskite solar cells, respectively. Hence the 400 nm thick solar cell reaches 92% of the theoretical short circuit current density limit of 25.6 mA/cm^2.

Acknowledgments

References

(1)   Li, Y.; Yan, W.; Li, Y.; Wang, S.; Wang, W.; Bian, Z.; Xiao, L.; Gong, Q. Direct Observation of Long Electron-Hole Diffusion Distance in CH3NH3PbI3 Perovskite Thin Film. *Sci. Rep.* **2015**, *5* (1), 14485. https://doi.org/10.1038/srep14485.

(2)   Wang, L.; Yuan, G. D.; Duan, R. F.; Huang, F.; Wei, T. B.; Liu, Z. Q.; Wang, J. X.; Li, J. M. Tunable Bandgap in Hybrid Perovskite CH3NH3Pb(Br3−yXy) Single Crystals and Photodetector Applications. *AIP Adv.* **2016**, *6* (4), 045115. https://doi.org/10.1063/1.4948312.

(3)   Castelli, I. E.; García-Lastra, J. M.; Thygesen, K. S.; Jacobsen, K. W. Bandgap Calculations and Trends of Organometal Halide Perovskites. *APL Mater.* **2014**, *2* (8), 081514. https://doi.org/10.1063/1.4893495.

(4)   Shi, D.; Adinolfi, V.; Comin, R.; Yuan, M.; Alarousu, E.; Buin, A.; Chen, Y.; Hoogland, S.; Rothenberger, A.; Katsiev, K.; et al. Low Trap-State Density and Long Carrier Diffusion in Organolead Trihalide Perovskite Single Crystals. *Science* **2015**, *347* (6221), 519–522. https://doi.org/10.1126/science.aaa2725.

(5)   Green, M. A.; Jiang, Y.; Soufiani, A. M.; Ho-Baillie, A. Optical Properties of Photovoltaic Organic–Inorganic Lead Halide Perovskites. *J. Phys. Chem. Lett.* **2015**, *6* (23), 4774–4785. https://doi.org/10.1021/acs.jpclett.5b01865.

(6)   Jiang, Y.; Green, M. A.; Sheng, R.; Ho-Baillie, A. Room Temperature Optical Properties of Organic–Inorganic Lead Halide Perovskites. *Sol. Energy Mater. Sol. Cells* **2015**, *137*, 253–257. https://doi.org/10.1016/j.solmat.2015.02.017.

(7)   Jang, S.; Yoon, J.; Ha, K.; Kim, M.; Kim, D. H.; Kim, S. M.; Kang, S. M.; Park, S. J.; Jung, H. S.; Choi, M. Facile Fabrication of Three-Dimensional TiO 2 Structures for Highly Efficient Perovskite Solar Cells. *Nano Energy* **2016**, *22*, 499–506. https://doi.org/10.1016/j.nanoen.2016.02.050.

(8)   Park, N.-G. Perovskite Solar Cells: An Emerging Photovoltaic Technology. *Mater. Today* **2015**, *18* (2), 65–72. https://doi.org/10.1016/j.mattod.2014.07.007.

(9)   Green, M. A.; Hishikawa, Y.; Dunlop, E. D.; Levi, D. H.; Hohl-Ebinger, J.; Ho-Baillie, A. W. Y. Solar Cell Efficiency Tables (Version 52). *Prog. Photovoltaics Res. Appl.* **2018**, *26* (7), 427–436. https://doi.org/10.1002/pip.3040.

(10)   Mailoa, J. P.; Bailie, C. D.; Johlin, E. C.; Hoke, E. T.; Akey, A. J.; Nguyen, W. H.; McGehee, M. D.; Buonassisi, T. A 2-Terminal Perovskite/Silicon Multijunction Solar Cell Enabled by a Silicon Tunnel Junction. *Appl. Phys. Lett.* **2015**, *106* (12), 121105. https://doi.org/10.1063/1.4914179.

(11)   Hörantner, M. T.; Leijtens, T.; Ziffer, M. E.; Eperon, G. E.; Christoforo, M. G.; McGehee, M. D.; Snaith, H. J. The Potential of Multijunction Perovskite Solar Cells. *ACS Energy Lett.* **2017**, *2* (10), 2506–2513. https://doi.org/10.1021/acsenergylett.7b00647.

(12)   Longo, G.; Momblona, C.; La-Placa, M.-G.; Gil-Escrig, L.; Sessolo, M.; Bolink, H. J. Fully Vacuum-Processed Wide Band Gap Mixed-Halide Perovskite Solar Cells. *ACS Energy Lett.* **2018**, *3* (1), 214–219. https://doi.org/10.1021/acsenergylett.7b01217.

(13)   Todorov, T. K.; Singh, S.; Bishop, D. M.; Gunawan, O.; Lee, Y. S.; Gershon, T. S.; Brew, K. W.; Antunez, P. D.; Haight, R. Ultrathin High Band Gap Solar Cells with Improved Efficiencies from the World's Oldest Photovoltaic Material. *Nat. Commun.* **2017**, *8* (1), 682. https://doi.org/10.1038/s41467-017-00582-9.

(14)   Chen, D.; Manley, P.; Tockhorn, P.; Eisenhauer, D.; Köppel, G.;

Hammerschmidt, M.; Burger, S.; Albrecht, S.; Becker, C.; Jäger, K. Nanophotonic Light Management for Perovskite-Silicon Tandem Solar Cells. *J. Photonics Energy* **2018**, *8* (2), 022601.

(15) Werner, J.; Sahli, F.; Fu, F.; Diaz Leon, J. J.; Walter, A.; Kamino, B. A.; Niesen, B.; Nicolay, S.; Jeangros, Q.; Ballif, C. Perovskite/Perovskite/Silicon Monolithic Triple-Junction Solar Cells with a Fully Textured Design. *ACS Energy Lett.* **2018**, *3* (9), 2052–2058. https://doi.org/10.1021/acsenergylett.8b01165.

(16) Shockley, W.; Queisser, H. J. Detailed Balance Limit of Efficiency of P-n Junction Solar Cells. *J. Appl. Phys.* **1961**, *32* (3), 510–519. https://doi.org/10.1063/1.1736034.

(17) Green, M. A.; Emery, K.; Hishikawa, Y.; Warta, W.; Dunlop, E. D. Solar Cell Efficiency Tables (Version 47). *Prog. Photovoltaics Res. Appl.* **2016**, *24* (1), 3–11. https://doi.org/10.1002/pip.2728.

(18) Sahli, F.; Werner, J.; Kamino, B. A.; Bräuninger, M.; Monnard, R.; Paviet-Salomon, B.; Barraud, L.; Ding, L.; Diaz Leon, J. J.; Sacchetto, D.; et al. Fully Textured Monolithic Perovskite/Silicon Tandem Solar Cells with 25.2% Power Conversion Efficiency. *Nat. Mater.* **2018**, *17* (9), 820–826. https://doi.org/10.1038/s41563-018-0115-4.

(19) Werner, J.; Niesen, B.; Ballif, C. Perovskite/Silicon Tandem Solar Cells: Marriage of Convenience or True Love Story? - An Overview. *Adv. Mater. Interfaces* **2018**, *5* (1), 1700731. https://doi.org/10.1002/admi.201700731.

(20) Bush, K. A.; Palmstrom, A. F.; Yu, Z. J.; Boccard, M.; Cheacharoen, R.; Mailoa, J. P.; McMeekin, D. P.; Hoye, R. L. Z.; Bailie, C. D.; Leijtens, T.; Peters, I. M.; Minichetti, M.C.; Rolston, N.; Prasanna R.; Sofia, S.; Harwood, D.; Ma, W.; Moghadam, F.; Snaith, H.J.; Buonassisi, T.; Holman, Z.C.; Bent, S.F.; MacGehee, M.D. 23.6%-Efficient Monolithic Perovskite/Silicon Tandem Solar

Cells with Improved Stability. *Nat. Energy* **2017**, *2* (4), 17009. https://doi.org/10.1038/nenergy.2017.9.

(21) Hossain, M. I.; Qarony, W.; Jovanov, V.; Tsang, Y. H.; Knipp, D. Nanophotonic Design of Perovskite/Silicon Tandem Solar Cells. *J. Mater. Chem. A* **2018**, *6* (8), 3625–3633. https://doi.org/10.1039/C8TA00628H.

(22) Jošt, M.; Köhnen, E.; Morales-Vilches, A. B.; Lipovšek, B.; Jäger, K.; Macco, B.; Al-Ashouri, A.; Krč, J.; Korte, L.; Rech, B.; Schlatmann, R.; Topič, M.; Stannowski, B.; Albrecht, S. Textured Interfaces in Monolithic Perovskite/Silicon Tandem Solar Cells: Advanced Light Management for Improved Efficiency and Energy Yield. *Energy Environ. Sci.* **2018**, *11* (12), 3511–3523. https://doi.org/10.1039/C8EE02469C.

(23) Forin, C. C.; Purica, M.; Budianu, E.; Schiopu, P. P-NiO/ITO Transparent Heterojunction - Preparation and Characterization. In *CAS 2012 (International Semiconductor Conference)*; IEEE, 2012; pp 131–134. https://doi.org/10.1109/SMICND.2012.6400676.

(24) Wang, J.-Y.; Lee, C.-Y.; Chen, Y.-T.; Chen, C.-T.; Chen, Y.-L.; Lin, C.-F.; Chen, Y.-F. Double Side Electroluminescence from P-NiO/n-ZnO Nanowire Heterojunctions. *Appl. Phys. Lett.* **2009**, *95* (13), 131117. https://doi.org/10.1063/1.3232244.

(25) You, J.; Meng, L.; Song, T.-B.; Guo, T.-F.; Yang, Y.; Chang, W.-H.; Hong, Z.; Chen, H.; Zhou, H.; Chen, Q.; Liu, Y.; De Marco, N.; Yang Y. Improved Air Stability of Perovskite Solar Cells via Solution-Processed Metal Oxide Transport Layers. *Nat. Nanotechnol.* **2016**, *11* (1), 75–81. https://doi.org/10.1038/nnano.2015.230.

(26) Müller, J.; Rech, B.; Springer, J.; Vanecek, M. TCO and Light Trapping in Silicon Thin Film Solar Cells. *Sol. Energy* **2004**, *77* (6), 917–930.

https://doi.org/10.1016/j.solener.2004.03.015.

(27) Dewan, R.; Owen, J. I.; Madzharov, D.; Jovanov, V.; Hupkes, J.; Knipp, D. Analyzing Nanotextured Transparent Conductive Oxides for Efficient Light Trapping in Silicon Thin Film Solar Cells. *Appl. Phys. Lett.* **2012**, *101* (10), 103903–103904.

(28) Hongsingthong, A.; Yunaz, I. A.; Miyajima, S.; Konagai, M. ZnO Films Prepared by Two-Step MOCVD Process for Use as Front TCO in Silicon-Based Thin Film Solar Cells. In *2010 35th IEEE Photovoltaic Specialists Conference,* IEEE **2010**, 001508–001511. https://doi.org/10.1109/PVSC.2010.5615836.

(29) Dikovska, A. O.; Atanasov, P. A.; Vasilev, C.; Dimitrov, I. G.; Stoyanchov, T. R. Thin ZnO Films Produced by Pulsed Laser Deposition. In *Journal of Optoelectronics and Advanced Materials* **2005**, 7, 1329–1334.

(30) Yoo, D.-G.; Nam, S.-H.; Kim, M. H.; Jeong, S. H.; Jee, H.-G.; Lee, H. J.; Lee, N.-E.; Hong, B. Y.; Kim, Y. J.; Jung, D.; Boo, J.-H. Fabrication of the ZnO Thin Films Using Wet-Chemical Etching Processes on Application for Organic Light Emitting Diode (OLED) Devices. *Surf. Coatings Technol.* **2008**, *202* (22–23), 5476–5479. https://doi.org/10.1016/j.surfcoat.2008.06.064.

(31) Hwang, K.-H.; Nam, S.-H.; Jung, W. S.; Lee, Y. M.; Yang, H.-S.; Boo, J.-H. Wet Chemical Etching of Al-Doped ZnO Film Deposited by RF Magnetron Sputtering Method on Textured Glass Substrate for Energy Application. *Bull. Korean Chem. Soc.* **2015**, *36* (3), 850–854. https://doi.org/10.1002/bkcs.10159.

(32) Makhlouf, A. S. H. Current and Advanced Coating Technologies for Industrial Applications. In *Nanocoatings and Ultra-Thin Films: Technologies and Applications* **2011**, 3–23. https://doi.org/10.1016/B978-1-84569-812-6.50001-4.

(33) Glass, A. Applied Glass Materials http://www.agc.com/en/products/applied_glass/index.html (accessed Aug 29,

2018).

(34) Jovanov, V.; Palanchoke, U.; Magnus, P.; Stiebig, H.; Hupkes, J.; Sichanugrist, P.; Konagai, M.; Wiesendanger, S.; Rockstuhl, C.; Knipp, D. Light Trapping in Periodically Textured Amorphous Silicon Thin Film Solar Cells Using Realistic Interface Morphologies. *Opt. Express* **2013**, *21* (13), A595–A606. https://doi.org/Doi 10.1364/Oe.21.00a595.

(35) Boccard, M.; Cuony, P.; Battaglia, C.; Hänni, S.; Nicolay, S.; Ding, L.; Benkhaira, M.; Bugnon, G.; Billet, A.; Charrière, M.; et al. Nanometer- and Micrometer-Scale Texturing for High-Efficiency Micromorph Thin-Film Silicon Solar Cells. *IEEE J. Photovoltaics* **2012**, *2* (2), 83–87. https://doi.org/10.1109/JPHOTOV.2011.2179414.

(36) Drude, P. Zur Elektronentheorie Der Metalle. *Ann. Phys.* **1900**, *306* (3), 566–613. https://doi.org/10.1002/andp.19003060312.

(37) Drude, P. Zur Elektronentheorie Der Metalle; II. Teil. Galvanomagnetische Und Thermomagnetische Effecte. *Ann. Phys.* **1900**, *308* (11), 369–402. https://doi.org/10.1002/andp.19003081102.

(38) Steinhauser, J. *PhD Thesis*; 2008.

(39) Löper, P.; Stuckelberger, M.; Niesen, B.; Werner, J.; Filipič, M.; Moon, S.-J.; Yum, J.-H.; Topič, M.; De Wolf, S.; Ballif, C. Complex Refractive Index Spectra of CH3NH3PbI3 Perovskite Thin Films Determined by Spectroscopic Ellipsometry and Spectrophotometry. *J. Phys. Chem. Lett.* **2015**, *6* (1), 66–71. https://doi.org/10.1021/jz502471h.

(40) Dewan, R.; Marinkovic, M.; Noriega, R.; Phadke, S.; Salleo, A.; Knipp, D. Light Trapping in Thin-Film Silicon Solar Cells with Submicron Surface Texture. *Opt. Express* **2009**, *17* (25), 23058. https://doi.org/10.1364/OE.17.023058.

(41) Parsons, R.; Tamang, A.; Jovanov, V.; Wagner, V.; Knipp, D. Comparison of

Light Trapping in Silicon Nanowire and Surface Textured Thin-Film Solar Cells. *Appl. Sci.* **2017**, *7* (4), 427. https://doi.org/10.3390/app7040427.

(42) Koida, T.; Fujiwara, H.; Kondo, M. Hydrogen-Doped In 2 O 3 as High-Mobility Transparent Conductive Oxide. *Jpn. J. Appl. Phys.* **2007**, *46* (No. 28), L685– L687. https://doi.org/10.1143/JJAP.46.L685.

(43) Barraud, L.; Holman, Z. C.; Badel, N.; Reiss, P.; Descoeudres, A.; Battaglia, C.; De Wolf, S.; Ballif, C. Hydrogen-Doped Indium Oxide/Indium Tin Oxide Bilayers for High-Efficiency Silicon Heterojunction Solar Cells. *Sol. Energy Mater. Sol. Cells* **2013**, *115*, 151–156. https://doi.org/10.1016/j.solmat.2013.03.024.
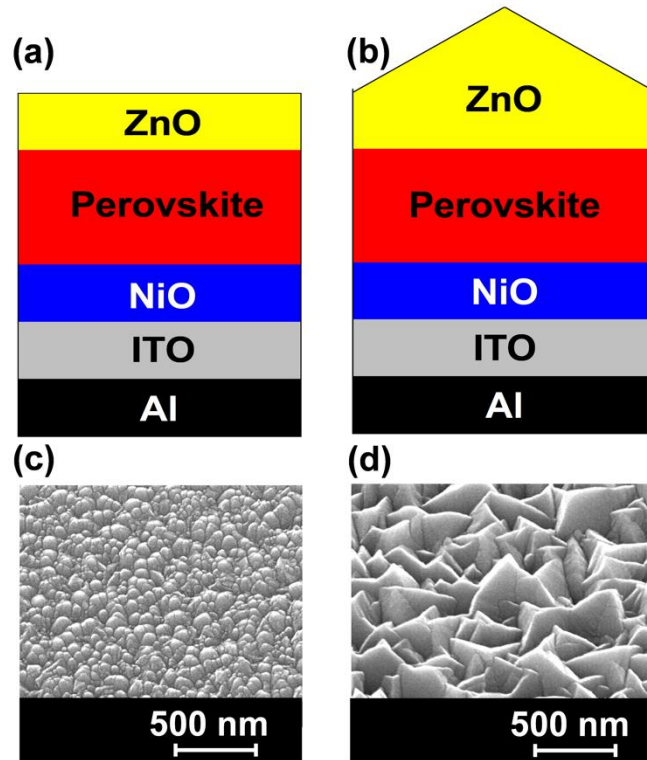
Figure 1*: Schematic cross-section of a perovskite solar cell with (a) planar and (b) textured zinc oxide front contacts. Corresponding SEM images of (c) smooth and (d) pyramidal textured ZnO films.*
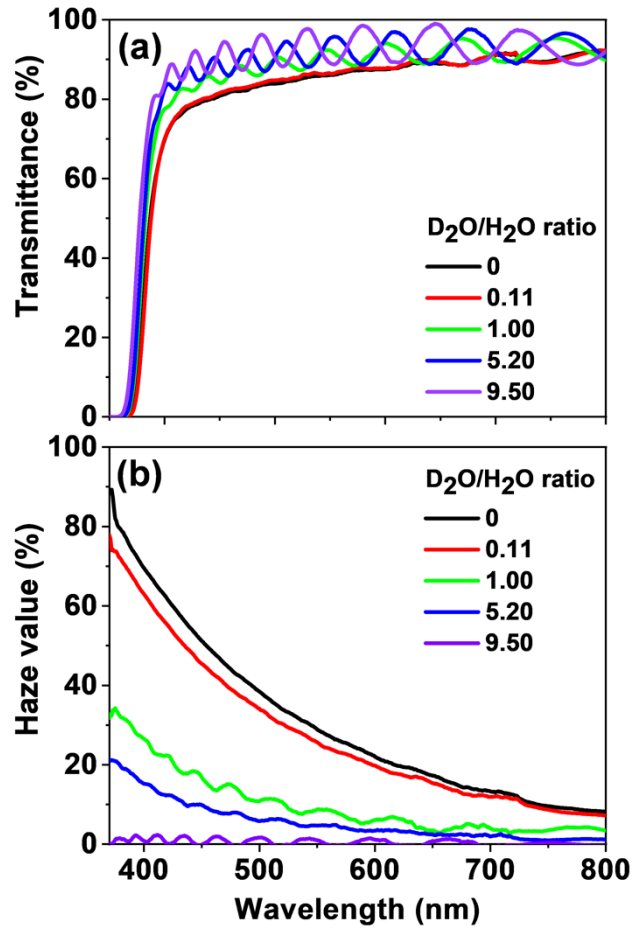
Figure 2: *(a) Measured total transmission of 1.6 µm thick ZnO film prepared by metal-organic chemical vapor deposition (MOCVD). The roughness of the film was varied by the D_2O/H_2O ratio during the growth process. The roughness increases with decreasing D_2O/H_2O ratio. (b) Haze in transmission. The haze is defined as the diffuse transmission normalized to the total transmission.*
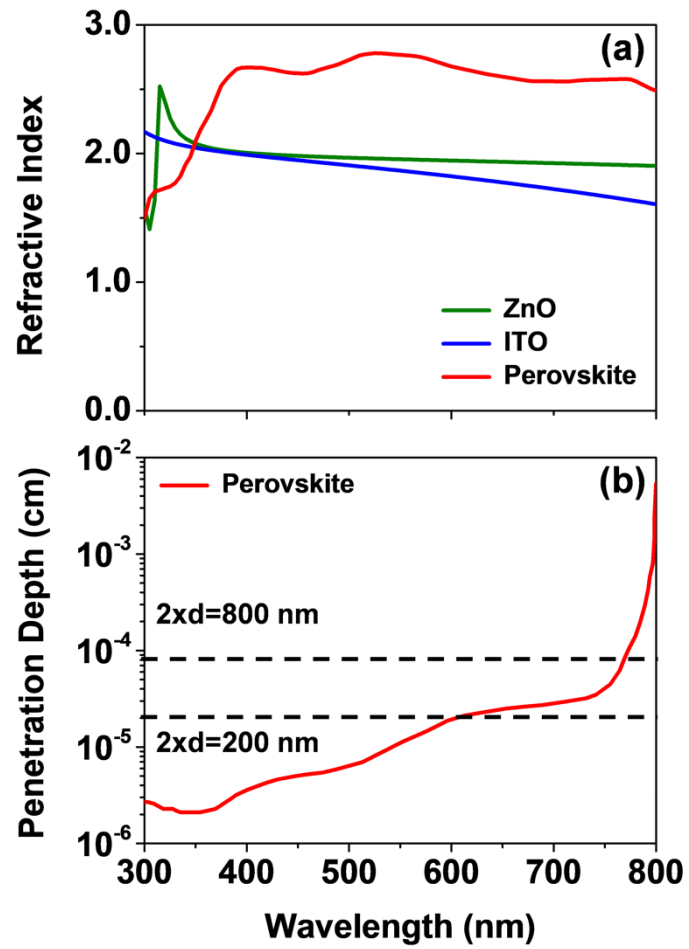
Figure 3: *(a) Refractive indices of ZnO, ITO, and Perovskite materials. (b) The penetration depth of the Perovskite material.*
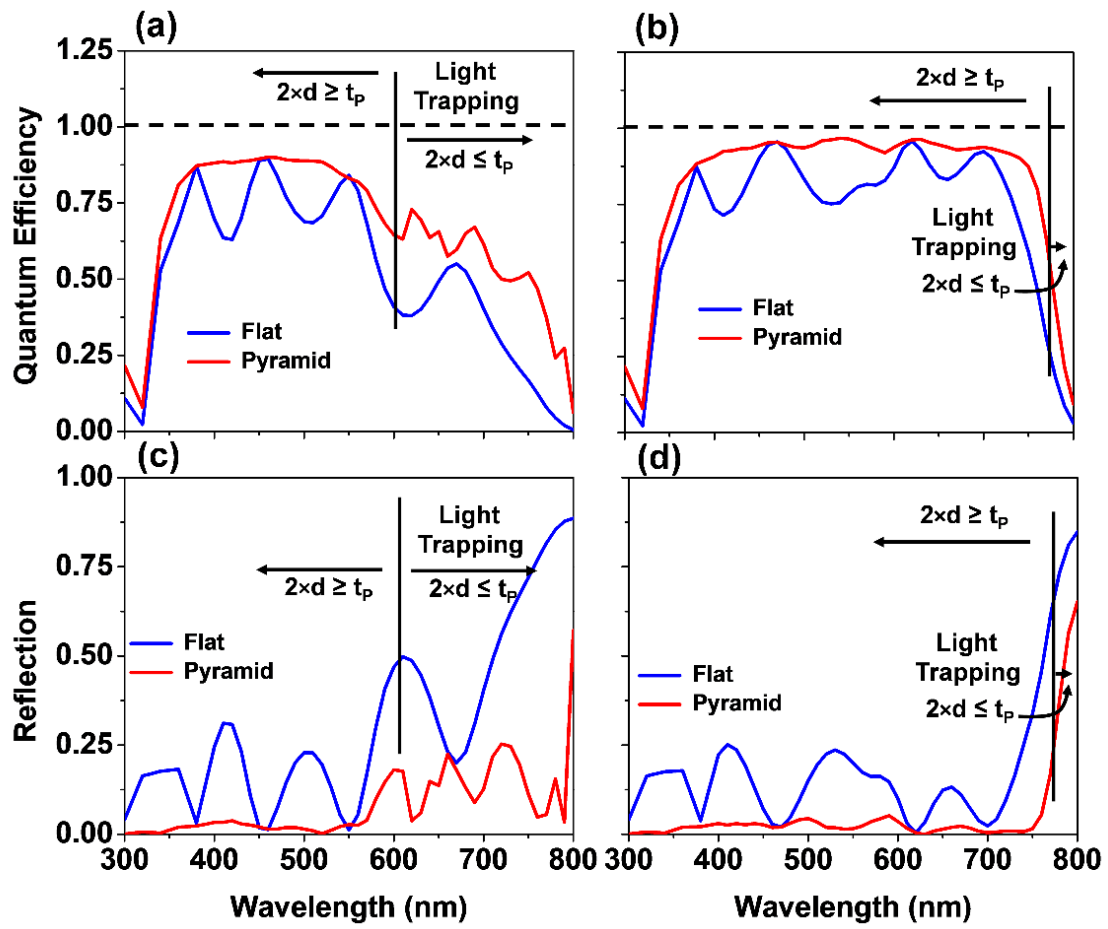
Figure 4: *Simulated quantum efficiency of flat and pyramidal textured perovskite solar cell with a period and height of 600 nm and 600 nm for a perovskite absorber layer thickness of (a) 100 nm and (b) 400 nm. Reflection of flat and pyramidal textured perovskite solar cell for a perovskite absorber layer thickness of (c) 100 nm and (d) 400 nm. (d and t_p are denoted as the perovskite absorber layer thickness and the penetration depth of perovskite material).*
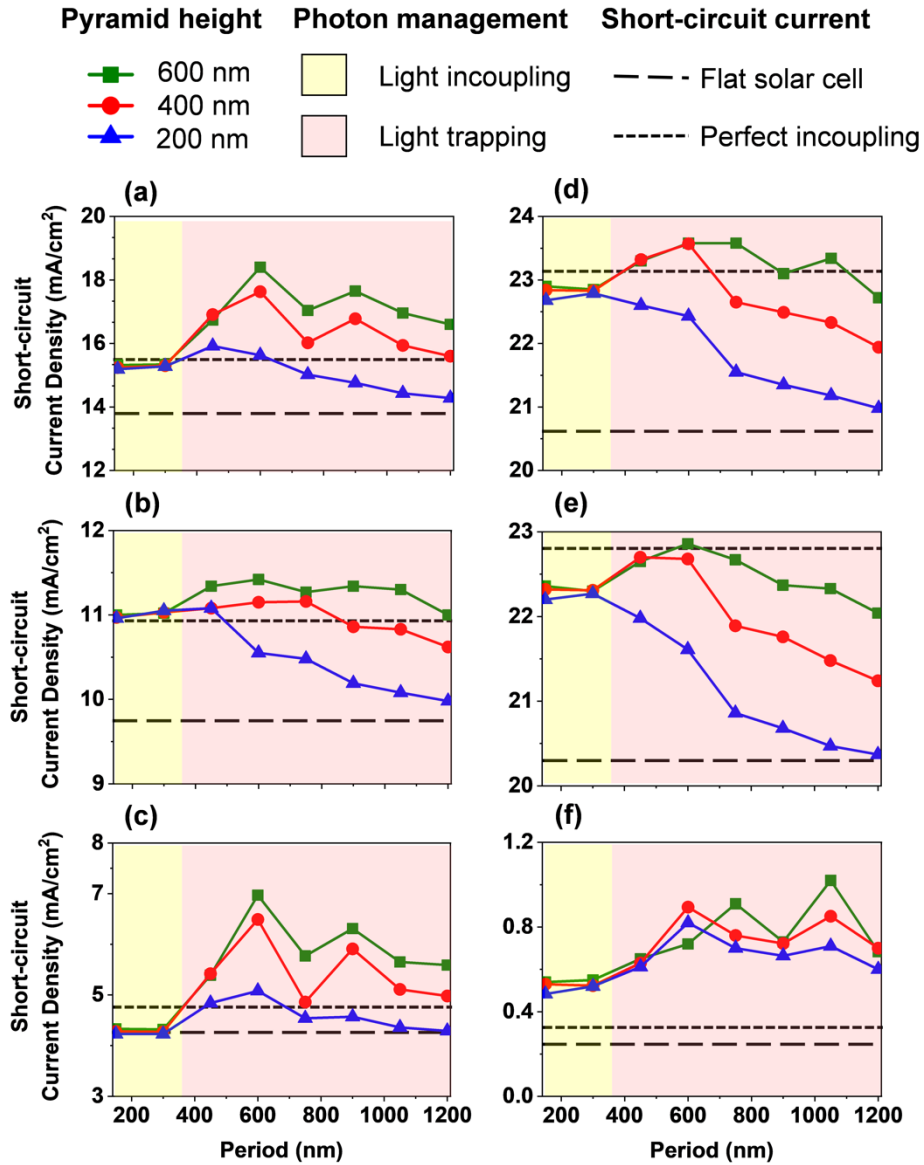
Figure 5: *Short-circuit current density for perovskite solar cells with absorber thickness of (a,b,c) 100 nm and (d,e,f) 400 nm as a function of the period of the front pyramidal surface texture. (a,d) Total short circuit current density and (b,e) short circuit current density up to the wavelength where the penetration depth is equal to twice the absorber thickness. (b) For the 100 nm thick perovskite solar cell the short circuit current is calculated from 300 nm to 610 nm, (e) while for the 400 nm thick perovskite solar cell the short circuit current is calculated from 300 nm to 770 nm. (c,f) Short circuit current density for wavelengths where the penetration depth is larger than twice the absorber thickness. (c) For the 100 nm thick perovskite solar cell the short circuit current is*

calculated from 610 nm to 800 nm, while for the 400 nm thick perovskite solar cell the short circuit current is calculated from 770 nm to 800 nm.
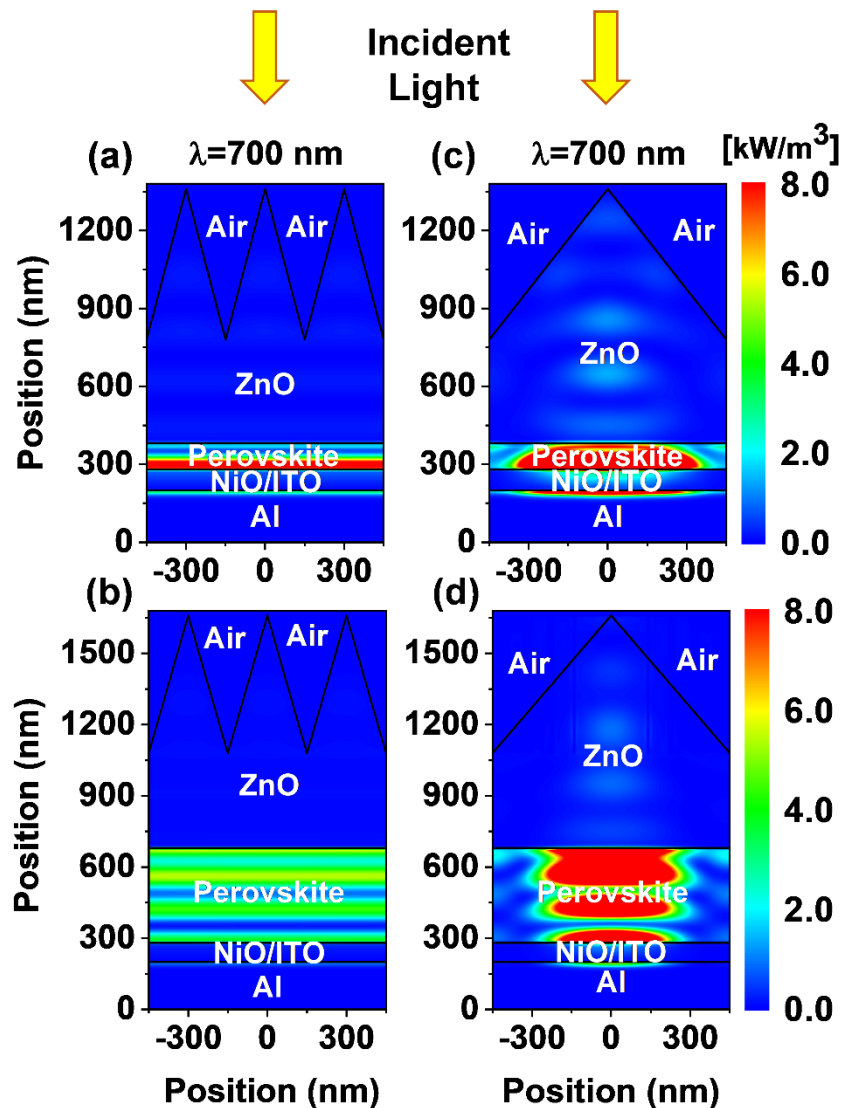

Figure 6: *Simulated power density profiles of perovskite solar cell with perovskite absorber layer thickness of (a,c) 100 nm and (b,d) 400 nm for a small and large period of (a,c) 300 nm and (b,d) 900 nm and fixed pyramid height of 600 nm, using an incident wavelength of 700 nm.*
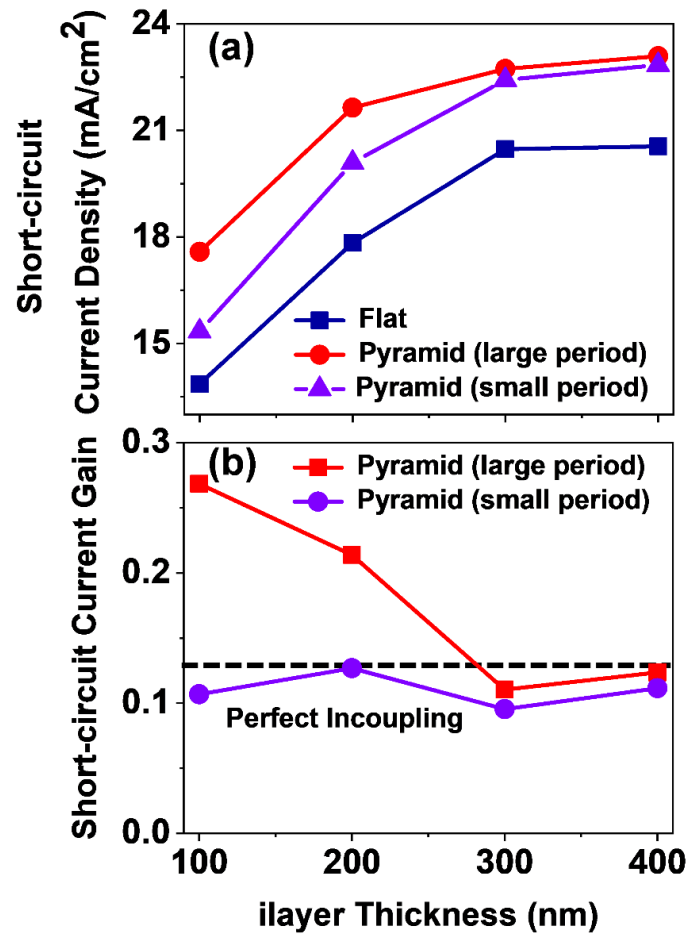
Figure 7: (a) A comparison of short-circuit current density among perovskite solar cells with a smooth surface, large period (900 nm), and a small period (300 nm). (b) A comparison of relative short-circuit current density gain between perovskite solar cell with large period (900 nm) and small period (300 nm).
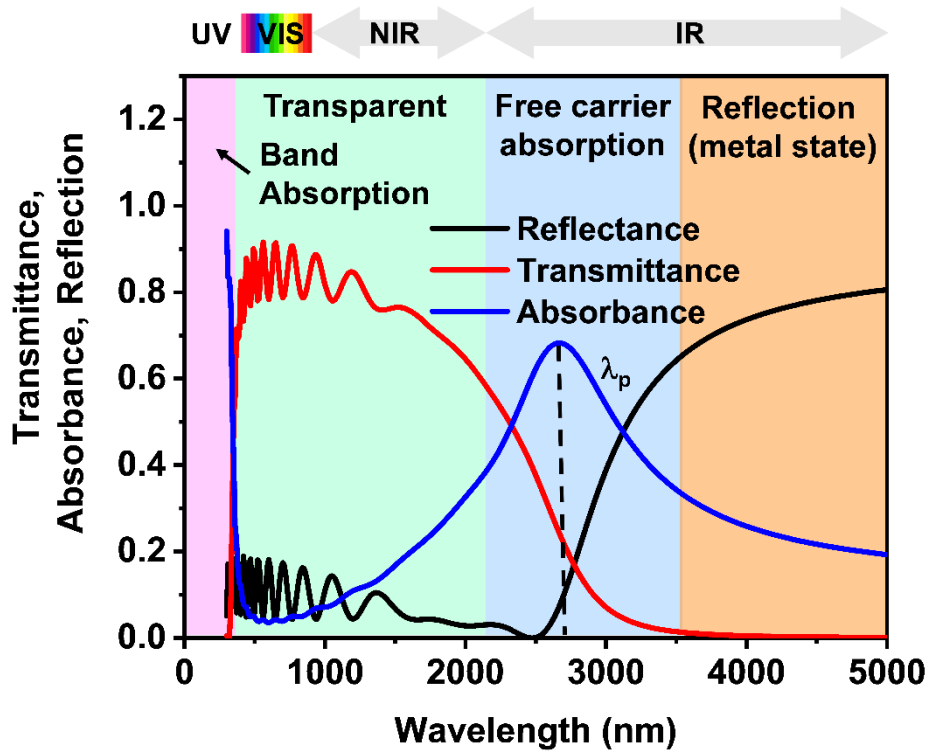
Figure 8*: The transmittance (T), absorbance (A), and reflectance (R) of a planar zinc oxide film.*
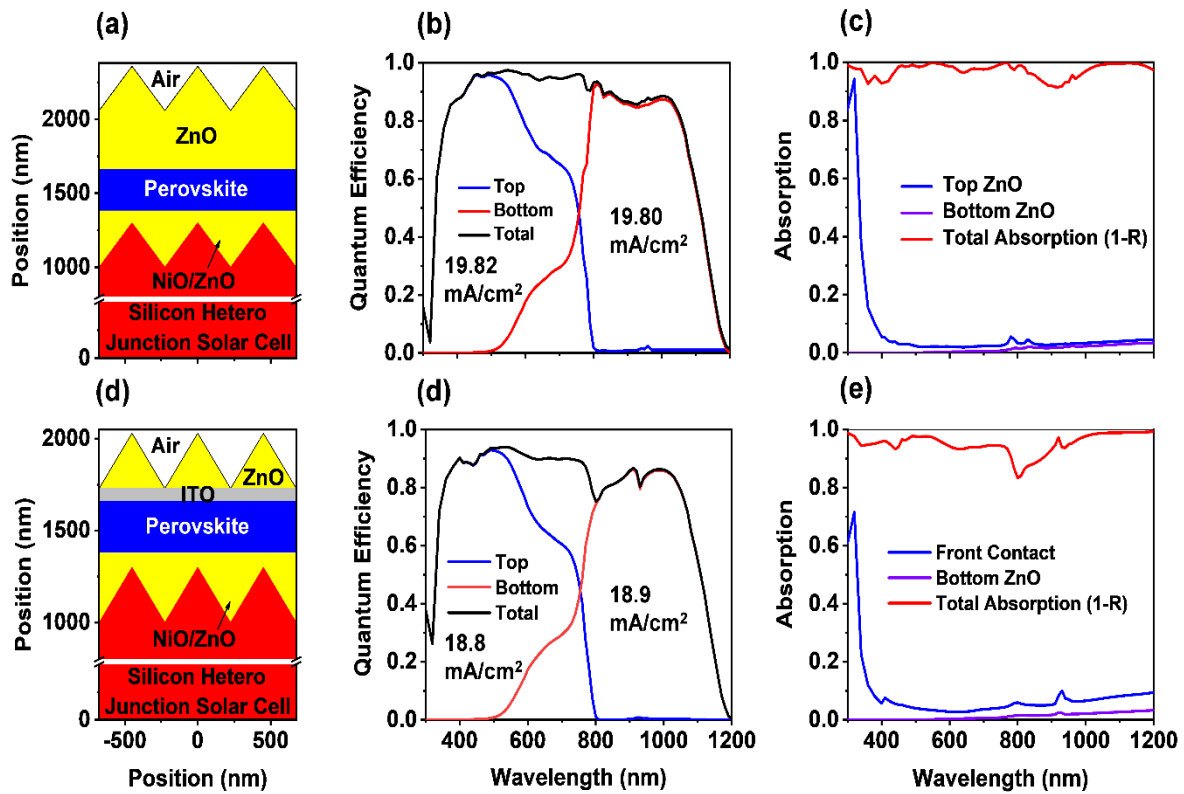
Figure 9: The schematic sketch of electrically flat and optically rough perovskite/silicon tandem solar cells with (a) a continuous front contact ZnO and (b) continuous ITO front contact. The corresponding quantum efficiency of the top and bottom cell and the total quantum efficiency are shown in (b,d). The total absorption (1-R) and the absorption of front and back contacts are also shown in (c,e).